Promotional Effect of Surface Plasmon Resonance on Direct Formation of Hydrogen Peroxide from H2 and O2 over Pd/Graphene-Au Nanorod Catalytic System

doi: 10.1016/j.jcat.2020.05.028

Promotional Effect of Surface Plasmon Resonance on Direct Formation of Hydrogen Peroxide from H_2 and O_2 over Pd/Graphene-Au Nanorod Catalytic System

Takeharu Yoshii,[1] *Yasutaka Kuwahara,*[1,2,3] *Kohsuke Mori,*[1,2] *and Hiromi Yamashita**[,1,2]

[1] Division of Materials and Manufacturing Science, Graduate School of Engineering, Osaka University, 2-1 Yamadaoka, Suita, Osaka 565-0871, Japan.

[2] Elements Strategy Initiative for Catalysts & Batteries Kyoto University (ESICB), Kyoto University, Katsura, Kyoto 615-8520, Japan.

[3] JST, PRESTO, 4-1-8 Honcho, Kawaguchi, Saitama 332-0012, Japan.

Corresponding Author

*E-mail: yamashita@mat.eng.osaka-u.ac.jp

Abstract

A promotional effect of surface plasmon resonance (SPR) on direct hydrogen peroxide (H_2O_2) formation from H_2 and O_2 over a structure-controlled Pd-Au catalytic system is reported herein. Pd NPs supported on reduced graphene oxide (rGO) layer-coated Au nanorod (NR) nanocomposite catalysts were synthesized, and the structure was confirmed by multiple characterization techniques. H_2O_2 production is highly enhanced under visible light irradiation in the direct H_2O_2 formation from H_2 and O_2. The H_2O_2 decomposition test and the H_2-D_2 exchange reaction reveal that the SPR of Au NRs facilitates H_2 activation on the Pd NP surface, leading to efficient H_2O_2 production. Furthermore, the rGO layer not only functions as an electron mediator in the catalytic reaction, but also contributes to the control of Pd NP sizes in the catalyst synthesis.

Keywords

Surface plasmon resonance

Hydrogen peroxide synthesis

Reduced graphene oxide

Gold nanorod

Heterogeneous catalysis

1. Introduction

Hydrogen peroxide (H_2O_2) is extensively utilized in industry as an environmentally friendly oxidant. At present, H_2O_2 is produced by an anthraquinone autooxidation method; however, the high energy requirement due to the multistep reaction process is a serious drawback.[1,2] The direct synthesis of H_2O_2 from H_2 and O_2 gases is conceptually the most straightforward process, and has attracted much attention as an alternative process with low energy consumption.[3–5] Pd-based catalysts have been known to efficiently produce H_2O_2 in the direct process.[6,7] However, Pd is also active for H_2O synthesis. Consequently, the produced H_2O_2 is easily converted to H_2O through decomposition and hydrogenation pathways, and therefore, achieving both activity improvement for H_2O_2 synthesis and suppression of H_2O_2 decomposition is needed.[8–11] In other words, the promotion of H_2 activation while preventing O-O bond dissociation is a key factor for efficient and selective H_2O_2 formation.[11-13] In order to enhance the H_2O_2 productivity, a number of Pd-based alloy catalysts have been studied, where electronic and geometric effect contributes to improve H_2O_2 selectivity or suppress H_2O_2 decomposition.[2,5,6,10-12] However, the selective H_2O_2 formation with Pd catalysts remains to be a challenging task despite a lot of efforts, and a new approach is desired.

Surface plasmon resonance (SPR), a photon-induced collective oscillation of electrons at the surface of noble metals, has lately come into focus in photocatalysis.[14-20] In photochemical processes, the excitation of SPR produces energetic hot electrons, which can be injected into specific orbitals of molecules adsorbed on the metal surface.[21,22] Specific reaction substrates and intermediates are activated, and thus, not only reaction rates, but also product selectivity can be controlled by the assistance of SPR.[23,24] N. J. Halas et al. have recently reported the SPR-induced dissociation of H_2 on Au NPs under visible light irradiation, in which hot electrons produced by the SPR of Au NPs can

be transferred into a contacted H_2 molecule.[25,26] On the basis of these studies, the SPR-driven H_2 activation could promote the direct H_2O_2 production from H_2 and O_2, without acceleration of H_2O_2 decomposition.

In this study, we present the promotional effect of SPR on the direct H_2O_2 formation from H_2 and O_2 over Pd nanoparticles deposited on graphene-Au nanorod (NR) nanocomposite catalysts. A large SPR-driven rate enhancement in the production of H_2O_2 is observed under visible light irradiation. It is demonstrated that the SPR of Au selectively facilitates H_2 activation, but not H_2O_2 decomposition on Pd, resulting in efficient H_2O_2 production. This study not only provides the first example of H_2O_2 production by assistance of SPR of Au NRs, but also offers design guidelines for developing plasmonic nanocomposite catalysts for selective H_2O_2 formation.

2. Experimental

2.1. Materials

Sulfuric acid (H_2SO_4), sodium nitrate ($NaNO_3$), potassium permanganate ($KMnO_4$), hydrogen peroxide (H_2O_2, 30%), hydrogen tetrachloroaurate(III) tetrahydrate ($HAuCl_4 \cdot 4H_2O$), sodium borohydride ($NaBH_4$), silver nitrate ($AgNO_3$), L(+)-ascorbic acid ($C_6H_8O_6$), disodium tetrachloropalladate(II) (Na_2PdCl_4), hydrochloric acid (HCl, 16.9%), disodium hydrogen phosphate dihydrate ($NaHPO_4$), citric acid, and perchloric acid ($HClO_4$, 60%) were purchased from Nacalai Tesque Inc. Cetyltrimethylammonium bromide ($C_{19}H_{42}BrN$) was purchased from Wako Pure Chemical Ind. Co., Ltd. Graphite powder and Oxo[5,10,15,20-tetra(4-pyridyl)porphinato]titanium(IV) ($[TiO(tpypH_4)]^{4+}$) were obtained from Kishida Chemical Co., Ltd and Tokyo Chemical Industry Co., Ltd, respectively. All chemicals were used without further purification.

2.2. Synthesis of PdNPs/Au@rGO

First, the graphene oxide (GO)-coated Au NR colloids (Au@GO) were prepared based on our previously reported methods.[27-29] Au NRs (aspect ratio = 3) were synthesized using a seed-mediated method, and nanosized GO suspension was prepared with a modified Hammer's method, followed by ultrasonication for exfoliation of GO sheets.[28] The Au NR colloids (98.0 mg/L, 20 mL) were centrifuged at 6000 rpm for 15 min to remove excess surfactant and the precipitants were re-dispersed in 20 mL of H_2O. The nanosized GO suspension (32.1 mg/L, 10 mL) was added to an Au NR colloid suspension (20 mL) and left at room temperature overnight. The obtained colloids are denoted as Au@GO.

In the next synthetic step, Pd nanoparticles (NPs) were formed on the carbon layer. A Na_2PdCl_4 solution (10 mM, 141 μL) was added to Au@GO and stirred for 15

min (denoted as Pd^{2+}/Au@GO). The prepared colloidal suspension was then reduced by continuous hydrogen bubbling through the suspension at 50 °C for 30 min. At the same time, the GO layer was partially reduced to reduced graphene oxide (rGO) to afford Pd NPs supported on rGO-coated Au NR colloids (denoted as PdNPs/Au@rGO). No sedimentation was observed in the colloidal suspension even after several months. The Pd content was calculated to be 7.2 wt% in PdNPs/Au@rGO.

2.3. Synthesis of reference catalysts

Reference catalysts were synthesized by a similar procedure as PdNPs/Au @rGO. PdNPs/rGO was synthesized by the impregnation of Na_2PdCl_4 solution (10 mM, 56.4 μL) on GO (20 mg) and the hydrogen reduction as described above (50 °C, 30 min). PdNPs/Au was prepared without the addition of the nanosized GO suspension in the PdNPs/Au@rGO synthesis.

2.4. Characterization

Transmission electron microscopy (TEM) images were obtained using a field emission-transmission electron microscope (FE-TEM; Hitachi Hf-2000) operated at 200 kV. Scanning transmission electron microscopy (STEM) images and elemental mappings were obtained using a JEOL-ARM 200F equipped with a Kvex energy-dispersive X-ray detector (JED-2300T) operated at 200 kV. Raman spectroscopy measurement was performed using a laser Raman confocal microscope (Nanophoton, RAMAN-11) using an excitation wavelength of 532 nm through a 20x objective. Colloidal samples were deposited on quartz slides, and then, dried under reduced pressure at room temperature. UV visible absorption spectra were examined using a Shimadzu UV-2600 UV-vis spectrophotometer with a quartz cell (light-path length = 1.0 cm) at room temperature. Pd

K-edge X-ray absorption fine structure (XAFS) spectra were recorded in fluorescence mode at 01B1 beamline at the SPring-8, JASRI, Harima, Japan, using a Si(111) monochromator. The Fourier transform was applied to the k^3-weighted normalized extended X-ray absorption fine structure (EXAFS) data over the range of $3.0 < k$ (Å^{-1}) < 12 to obtain radial structure functions using a Rigaku software REX2000. The zeta potential was measured using a zeta potential analyzer (Otsuka Electronics Co., Ltd., ELSZ-2000). The pH of each suspension was adjusted to 6 by using McIlvaine buffer solution.

2.5. Catalytic test

The catalytic performance was evaluated by the direct hydrogen peroxide formation from hydrogen and oxygen. In a typical procedure, the colloidal suspension containing catalyst (10 mL) and HCl (1 mol/L, 100 μL) were added into a glass reactor for pH adjustment. The reactor was placed in a water bath at 15 °C under continuous stirring in the dark or under visible light irradiation (500 W Xe lamp (SAN-EI ELECTRIC Co., Ltd., XEF-501S) with a 420 nm long-pass filter), and the reaction was initiated by bubbling a gas mixture containing hydrogen gas (10 mL/min) and oxygen gas (10 mL/min) through the suspension. The visible-light intensity was set to I = 120 mW/cm^2. The amount of produced H_2O_2 was examined by spectroscopic titration with an acidic solution of $[TiO(tpypH_4)]^{4+}$ complex (TiP reagent).[30] The TiP reagent was prepared by dissolving the $[TiO(tpypH_4)]^{4+}$ complex (3.4 mg) in 100 mL of 50 mM hydrochloric acid. An aliquot of the reaction solution was diluted with water and used as the sample solution, and then 250 μL of the sample solution, 250 μL of 4.8 M perchloric acid, and 250 μL of the TiP reagent were mixed. After 2 min, the mixture was diluted to 2.5 mL with water and used for the spectroscopic measurements. Absorbance at λ = 432 nm was measured

using a Shimadzu UV-2600 UV-Vis spectrophotometer (AS). A blank solution was prepared by adding water instead of the sample solution, and its absorbance was designated as AB. The difference in absorbance was determined by the following equation: $\Delta A_{432} = AB - AS$. Based on ΔA_{432} and the volume of the solution, the produced amount of H_2O_2 was determined using a calibration curve prepared in advance.[31]

The H_2O_2 hydrogenation test was carried out as follows. The suspension containing a colloidal catalyst (10 mL) and HCl (1 mol/L, 100 μL) were added into a glass tube. The glass tube was placed in a water bath at 15 °C, and Ar gas (10 mL/min) was bubbled through the suspension. The reaction was initiated by addition of a designated amount of H_2O_2 with bubbling of hydrogen gas (10 mL/min) under continuous stirring in the dark or under visible light irradiation ($\lambda > 420$ nm, $I = 120$ mW/cm^2). A H_2O_2 decomposition test was also performed without the hydrogen gas bubbling for the hydrogenation test of H_2O_2.

2.6. H_2-D_2 exchange reactions

The colloidal suspension of prepared catalyst (5 mL) was added into a glass reactor, which was placed in an oil bath at 30 °C under continuous stirring in the dark or under visible light irradiation (500 W Xe lamp (SAN-EI ELECTRIC Co., Ltd., XEF-501S) with a 420 nm long-pass filter).[25,32] A mixed gas containing H_2 gas (1 mL/min), deuterium (D_2) gas (1 mL/min), and Ar gas (4 mL/min) was bubbled through the suspension. To analyze the HD production rate, the outlet gas was examined by gas chromatography (Shimadzu GC-2014 instrument) with He as the carrier gas and a Shinwa OGO–SP column held at -196 °C, in conjunction with a thermal conductivity detector.[33,34] All results were deducted of a background HD measured using pure water instead of the colloidal suspension.

3. Results and Discussion

3.1. Synthesis and characterization of PdNPs/Au@GO

The colloidal catalysts of Pd NPs supported on rGO-coated Au NRs (PdNPs/Au@rGO) were synthesized by a bottom-up method. In this nanocomposite structure, the SPR of Au nanorods is excited by a wide range of visible light because of the anisotropic structure, and hot-electrons concentrated at the ends of the long axis can be efficiently utilized for the catalytic reaction promotion.[35,36] In addition, the contacted rGO layer contributes to efficient transportation of hot-electrons from the surface of Au NRs to the Pd active sites.[28] First, graphene oxide (GO)-coated Au nanorods (Au@GO) were prepared based on our recently reported method.[28] The size of GO, synthesized by a modified Hummer's method,[37] was reduced through sonication and filtration to yield the nanosized GO suspension.[29] Then, colloidal Au NRs (Figure 1A; 25 nm diameter, 75 nm length, aspect ratio = 3) and the prepared nanosized GO suspension were mixed to yield Au@GO. The homogeneous coating of the GO layer on the Au NR surface was confirmed in the TEM image (Figure 1B). As shown in Figure S1, the surface charge of Au NRs was positive (zeta protentional = 39.0). In contrast, the surface of the nanosized GO was negatively charged (zeta protentional = -29.0), owing to the carboxylic acid and phenolic hydroxy groups on the surface of GO. Since Au NRs and the nanosized GO were oppositely charged, there should be an interaction between Au NRs and the nanosized GO. In addition, the zeta potential of Au@GO was 29.4, which was between that of Au NRs and the nanosized GO, indicating the formation of the nanocomposite material due to the electrostatic interaction.

In the next step, Na_2PdCl_4 aqueous solution was added to the Au@GO colloidal suspension (denoted as Pd^{2+}/Au@GO), and hydrogen gas was bubbled through the suspension at 50 °C to form Pd NPs on the layer. At the same time, the GO layer was

partially reduced, and the final product of PdNPs/Au@rGO was obtained. Figures 1C and 1D present TEM images of PdNPs/Au@rGO, where Pd NPs (circled in Figure 1D) with a mean diameter of 4.2 nm having a narrow size distribution are observed on the rGO layer. It is noted that the size distribution of NPs was analyzed using multiple STEM and TEM images with a wider range (Figure S2).

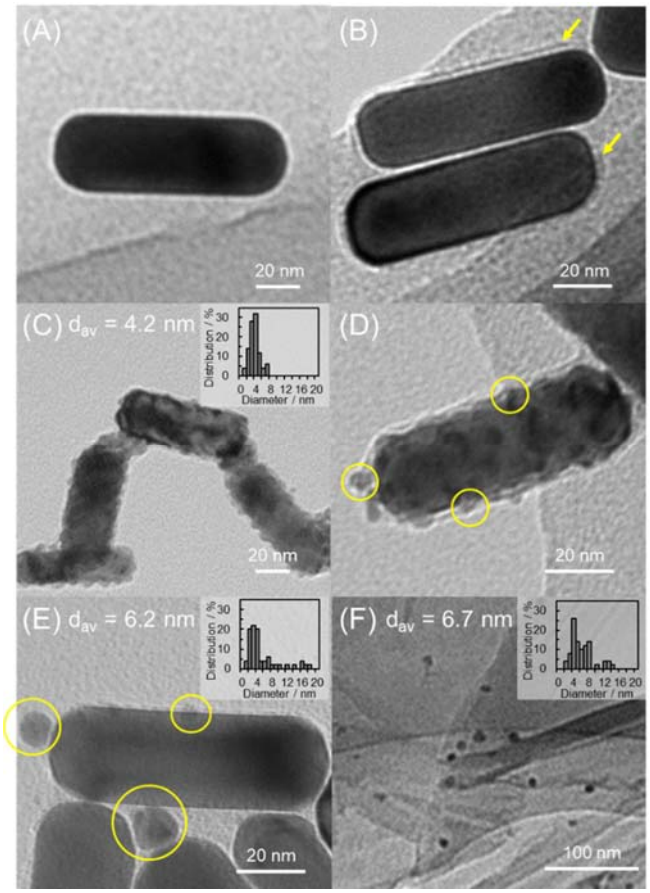

Figure 1 TEM images of (A) Au NR colloids, (B) Au@rGO, (C, D) PdNPs/Au@rGO, (E) PdNPs/Au, and (F) PdNPs/rGO. Insets in (C, E, F) show distributions of Pd NPs in each TEM image.

Scanning transmission electron microscopy (STEM) and corresponding EDX elemental mapping images (Figure 2) reveal that the Au NRs are homogeneously surrounded by the rGO layer, and the NPs deposited on the rGO layer consist of Pd species (see also EDX spectra in Figure S3). TEM images of the reference catalysts of PdNPs/Au and PdNPs/GO are shown in Figures 1E and 1F, respectively. In contrast to PdNPs/Au@rGO, the Pd species in PdNPs/Au were randomly aggregated to create large NPs with a mean diameter of 6.2 nm, whose size distribution is much broader than that for PdNPs/Au@rGO (see Figure 1C). In addition, the TEM image of PdNPs/rGO showed NPs having a mean diameter of 6.7 nm with a narrow size distribution on the rGO surface. Since the pristine, not exfoliated, GO was utilized as a support for PdNPs/rGO, the NP size of PdNPs/rGO was larger than that of PdNPs/Au@rGO, but the Pd NPs on both PdNPs/rGO and PdNPs/Au@rGO were uniformly deposited. Considering these results, GO contributes to the control of the size of metal NPs, which enables the uniform formation of Pd NPs in the PdNPs/Au@rGO catalyst.

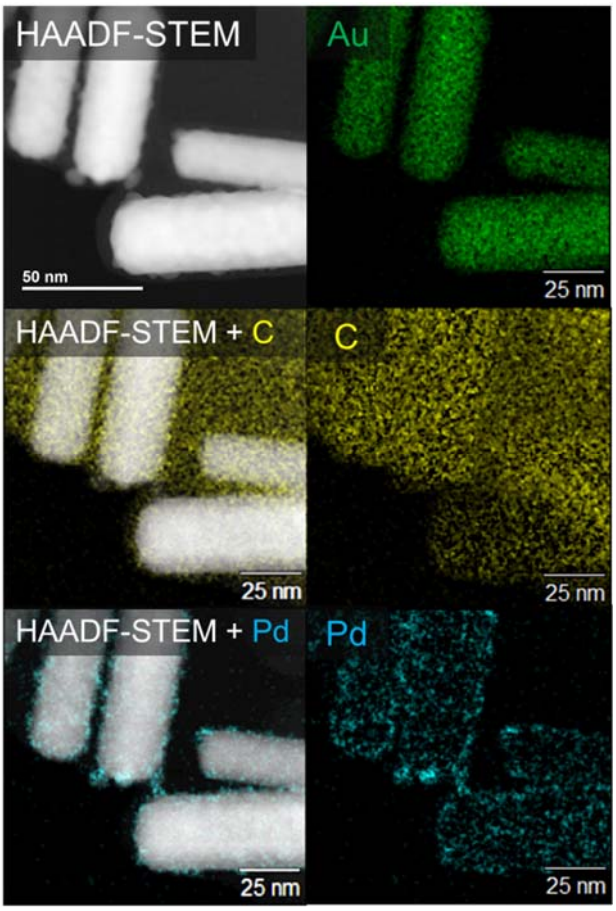

Figure 2 HAADF-STEM images and EDX mapping images of PdNPs/Au@rGO. Note: C signals in the upper-right of the figure are derived from the grid for the STEM observation.

Figure 3 shows the UV-vis absorption spectra of prepared samples: colloidal Au NRs, Au@GO, Pd^{2+}/Au@GO, and PdNPs/Au@rGO. Even after the GO layer coating, visible light absorption bands are retained at the wavelengths of 520 and 720 nm assigned to the SPR of the anisotropic Au NRs.[38] In addition, a new absorption band at around 260 nm in Au@GO indicates the presence of the GO layer. The absorption bands of Pd^{2+} ions in the UV region shown in Pd^{2+}/Au@GO disappear after hydrogen treatment, which reveals the complete reduction of Pd^{2+} ions to the Pd NPs on the rGO layer. The formation

of Pd NPs through the hydrogen treatment was also confirmed by the color change of the suspension from dark-red to black as shown in the inset of Figure 3.

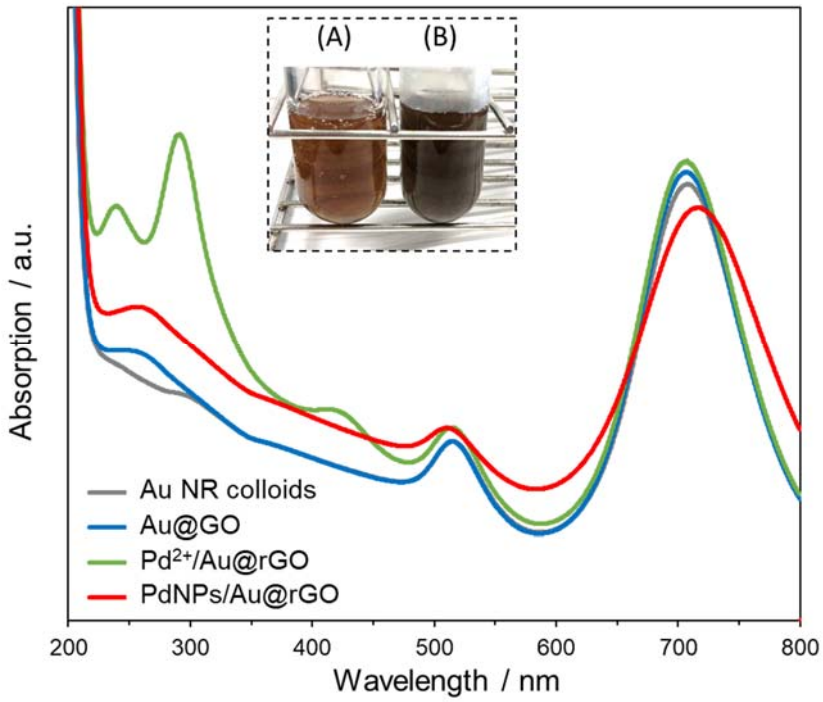

Figure 3 UV-vis spectra of Au NR colloids, Au@GO, Pd^{2+}/Au@rGO, and PdNPs/Au@rGO. Inset: Images of (A) Pd^{2+}/Au@rGO and (B) PdNPs/Au@rGO.

X-ray absorption structure (XAFS) measurements were performed to examine the state of the Pd species. The Pd K-edge X-ray absorption near-edge structure (XANES) spectra of all prepared samples are similar to those for Pd foil (Figure S4A). In addition, Fourier transform extended X-ray absorption structure (EXAFS) spectra exhibit a strong peak at around 2.6 Å, assignable to Pd–Pd bonds, revealing the complete reduction of Pd^{2+} ions to metallic Pd NPs, consistent with the UV-vis results (Figure S4B).

The reduction of the GO layer to rGO through hydrogen treatment was confirmed by Raman spectroscopy. The bands in the Raman spectra at around 1355 and

1593 cm^{-1} are associated with the D band and G band, respectively, and the intensity ratio (I_D/I_G) indicates the degree of reduction of GO; I_D/I_G increases along with the reduction of GO to rGO.[39,40] Figure S5 summarizes the Raman spectra of prepared samples with the intensity ratio (I_D/I_G). The I_D/I_G of GO slightly increases to 0.99 through the sonication process (see Figures S5a and S5b), and the degree of reduction in nanosized GO is maintained even after being combined with Au NRs (Figure S5c). PdNPs/Au@rGO (Figure S5d) presents a higher I_D/I_G than Au@GO, demonstrating the reduction of the GO layer to electro-conductive rGO through hydrogen treatment, along with the formation of Pd NPs. In addition, the reduction of GO was confirmed in the PdNPs/rGO synthesis (Figure S5e).

3.2. Direct H_2O_2 formation from H_2 and O_2

The catalytic performance of the prepared samples was assessed in the direct H_2O_2 formation from H_2 and O_2. In the reaction, Pd catalyzes H_2O_2 formation from H_2 and O_2 (eq. (1)), but at the same time, a competing reaction of H_2O production also occurs (eq. (2)).

$$H_2 + O_2 \rightarrow H_2O_2 \quad (1)$$

$$H_2 + 1/2O_2 \rightarrow H_2O \quad (2)$$

In addition, since H_2O_2 is thermodynamically unstable compared to H_2O, the produced H_2O_2 is easily converted to H_2O through both self-decomposition (eq. (3)) and over-hydrogenation (eq. (4)) pathways on the Pd surface.

$$H_2O_2 \rightarrow H_2O + 1/2O_2 \quad (3)$$

$$H_2O_2 + H_2 \rightarrow 2H_2O \quad (4)$$

Therefore, the H_2O_2 concentration is determined from the balance of these four reactions.[5,41] Figure 4A shows the time course of the direct H_2O_2 formation using

PdNPs/Au@rGO under visible light irradiation ($\lambda > 420$ nm) and in the dark at 15 °C. H_2O_2 concentration first increased to 30 μmol/L in the dark, but it remained at around 25 μmol/L after 30 min of reaction, due to the reaction equilibrium between H_2O_2 production and decomposition. In contrast, H_2O_2 was promptly produced under visible light irradiation, and the H_2O_2 concentration was highly enhanced to around 160 μmol/L. After 4 h, the reaction was changed to the dark condition, whereupon the H_2O_2 concentration smoothly fell to 50 μmol/L, clearly indicating that the H_2O_2 formation was promoted by the assistance of light irradiation. Considering the fact that GO-coated Au NR colloids (Au@rGO) synthesized without Pd species showed no activity in Figure 4C, Pd NPs served as active sites for H_2O_2 formation in PdNPs/Au@rGO. The rGO-supported Pd NPs (PdNPs/rGO) exhibited no production enhancement under visible light irradiation, and thus, the SPR of Au NRs under visible light irradiation contributed to the improvement of H_2O_2 production over the Pd surface in the PdNPs/Au@rGO (Figure 4B). It should be noted that the state of the Pd species did not change even after the reaction under both visible light and in the dark (see Figures S4d and S4e). When the sample without the rGO layer (PdNPs/Au) was employed, the enhancement rate under visible light was only 1.6, which is inferior to that for PdNPs/Au@rGO (Figure 4B). As presented in the TEM image of Figure 1E, Pd NPs were formed randomly in irregular sizes in PdNPs/Au, and therefore, the controlled deposition of Pd species on the rGO layer in PdNPs/Au@rGO is an important factor for the SPR-driven highly efficient H_2O_2 production. The impact of the size of the Pd species on the catalytic activity was further investigated. As shown in Figure 4C, the H_2O_2 production was enhanced as the amount of introduced Pd species increased to 7.2 wt%, whereas the sample having 9.8 wt% Pd exhibited lower activity than the sample with 7.2 wt% Pd. By comparing TEM images of the samples with different amounts of Pd species (Figures S6A and S6B), the sample with higher Pd content

was found to have a larger size of Pd NPs. Therefore, the H_2O_2 production is largely affected by the size of NPs, and the optimum size is considered to be 6.2 nm. Summarizing these results, the SPR of Au NRs can efficiently promote H_2O_2 formation on Pd species in the structure-controlled rGO-Au NRs supported Pd NP catalysts.

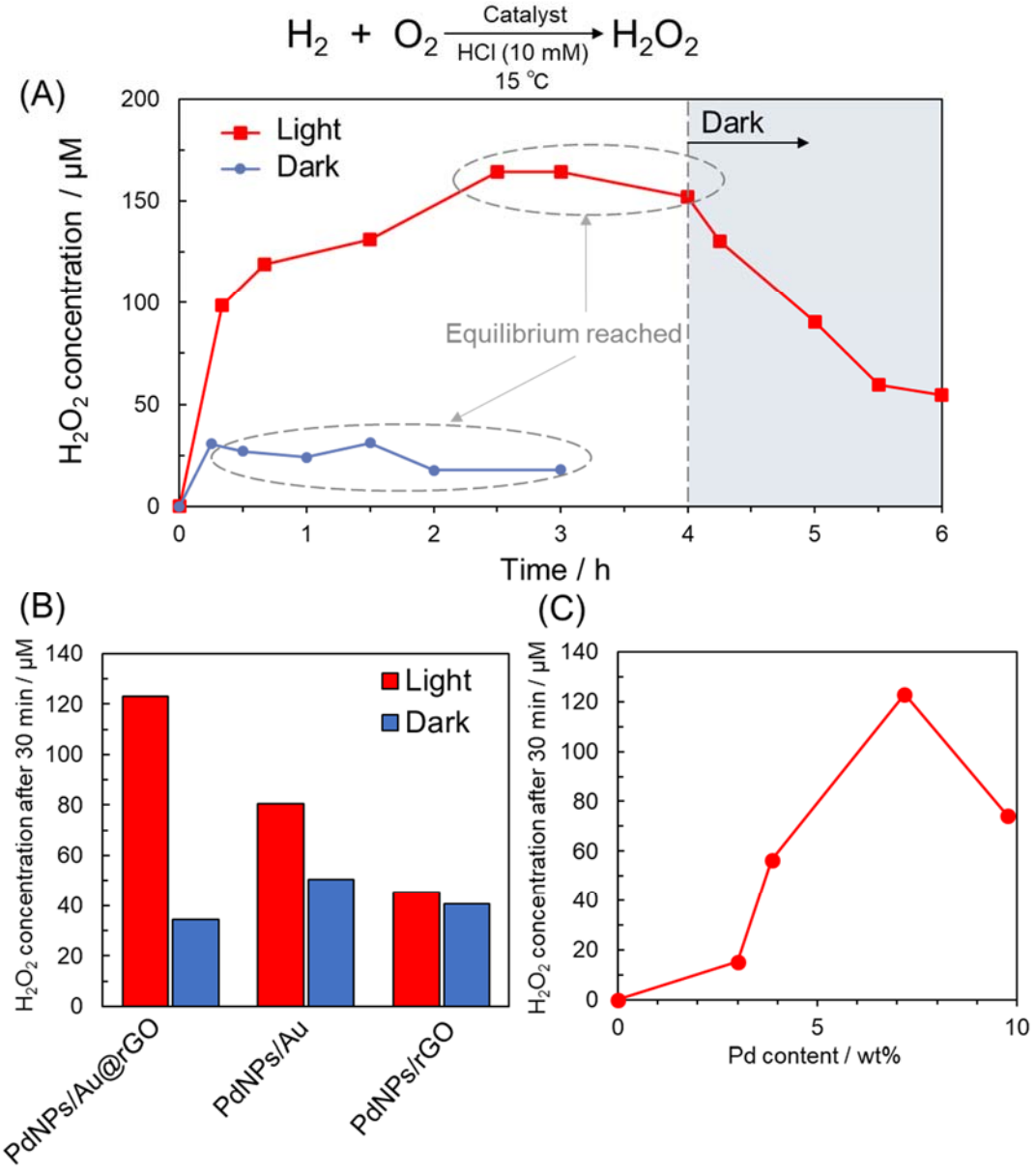

Figure 4 (A) Time course in the direct H_2O_2 formation from H_2 and O_2 under visible light irradiation (red line) and in the dark (blue line). Note: After 4 h under visible light irradiation, the reaction was changed to the dark condition. Comparison of catalytic

activity in the direct H_2O_2 formation under visible light irradiation (B) over PdNPs/Au@rGO, PdNPs/Au, and PdNPs/rGO under visible light irradiation and in the dark, and (C) over PdNPs/Au@rGO with different Pd contents under visible light irradiation.

3.3. Reaction promotion mechanism in the direct H_2O_2 formation by surface plasmon resonance

There are two possible effects of the SPR of Au NRs on the enhancement of the H_2O_2 production: 1) improving the activity for the H_2O_2 formation reaction from H_2 and O_2, and 2) suppressing the decomposition of produced H_2O_2 to H_2O. To elucidate the origin of the reaction promotion in PdNPs/Au@rGO, the H_2O_2 decomposition rate was examined. As mentioned in the previous section, H_2O_2 can be converted to H_2O through two pathways: self-decomposition (eq. (3)) and over-hydrogenation (eq. (4)). Thus, the self-decomposition test of H_2O_2 (eq. (3)) was first conducted.

As shown in Figure 5A, only a little promotion of decomposition was observed under visible light irradiation compared to that in the dark. H_2O_2 did not decompose without any catalyst, suggesting that the self-decomposition occurs on the Pd surface in the catalyst. On the other hand, the H_2O_2 decomposition under H_2 bubbling was doubled under visible light irradiation, which demonstrated the promotional effect of the SPR of Au NRs on the over-hydrogenation of H_2O_2 to H_2O (eq. (4)) (Figure 5B). In the over-hydrogenation pathway, firstly H_2 was activated on the Pd surface, and the H_2O_2 was hydrogenated by the activated H_2 to form H_2O.[11,12] Therefore, the reaction result indicates that the H_2 activation on the Pd surface was promoted by SPR of Au NRs. Here, the H_2O_2 formation also proceeds through the hydrogenation pathway (eq. (1)), and the acceleration of H_2 activation by the assist of the SPR of Au NRs leads to the promotion

of H_2O_2 production. Therefore, these results not only refute the hypothesis of SPR-driven suppression of H_2O_2 decomposition, but also imply that the H_2O_2 formation reaction (eq. (1)) is boosted by the SPR of Au NRs, because only the hydrogenation route (eq. (4)) was accelerated under visible light irradiation among the two decomposition pathways (eqs. (3) and (4)).

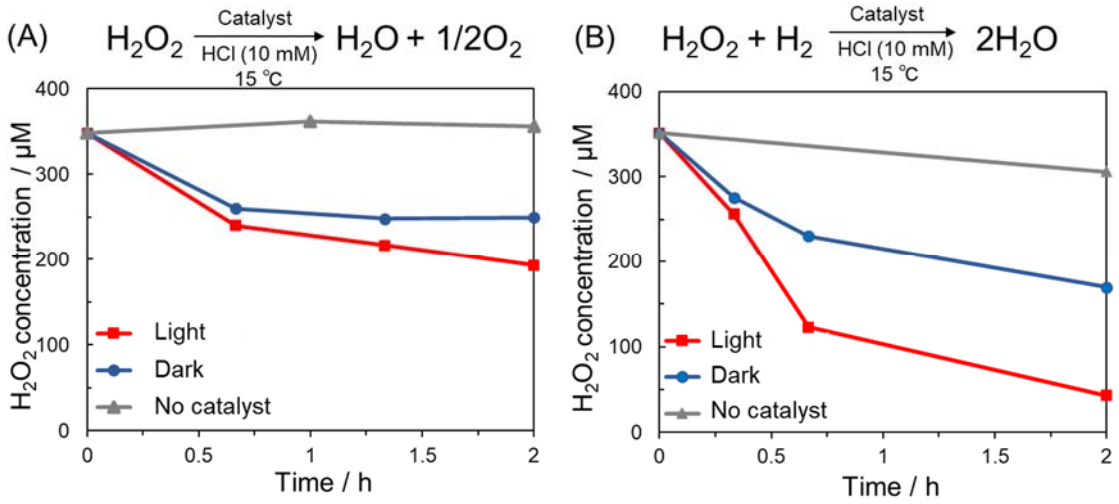

Figure 5 Time courses (A) in the H_2O_2 self-decomposition test and (B) in the H_2O_2 hydrogenation test under visible light irradiation and in the dark condition using PdNPs/Au@rGO as a catalyst.

To gain further insight into the reaction promotion mechanism, the rate of H_2 activation was examined through the H_2-D_2 exchange reaction. The HD production rate was measured with H_2 and D_2 gases bubbling through the suspension containing PdNPs/Au@rGO under visible light irradiation and in the dark. Figure 6 exhibits the time course of the HD production rate, showing a significant activity increase under visible light irradiation. The catalyst without Pd NPs (Au@rGO) provides no catalytic performance for the H_2-D_2 exchange reaction even under light irradiation. Therefore, Pd species act as the active sites in PdNPs/Au@rGO, and the reaction acceleration is driven by the SPR of Au NRs. Previous reports also demonstrated the SPR-mediated H_2

activation over Au NPs supported on SiO_2, where hot electrons generated by the SPR induced the H_2 dissociation on Au NPs.[25,26] In addition, we previously reported that the rGO layer functioned as a hot-electron mediator between plasmonic Au NRs and catalytically active Pd species.[28] Based on these studies, the hot electrons produced by the SPR in Au NRs are transferred to the Pd NPs *via* the rGO layer in PdNPs/Au@rGO, promoting H_2 activation on the Pd surface. Since the H_2 activation ability directly relates to the H_2O_2 production performance (eq. (1)), the SPR-enhanced H_2 activation leads to the large H_2O_2 production of PdNPs/Au@rGO under visible light irradiation.

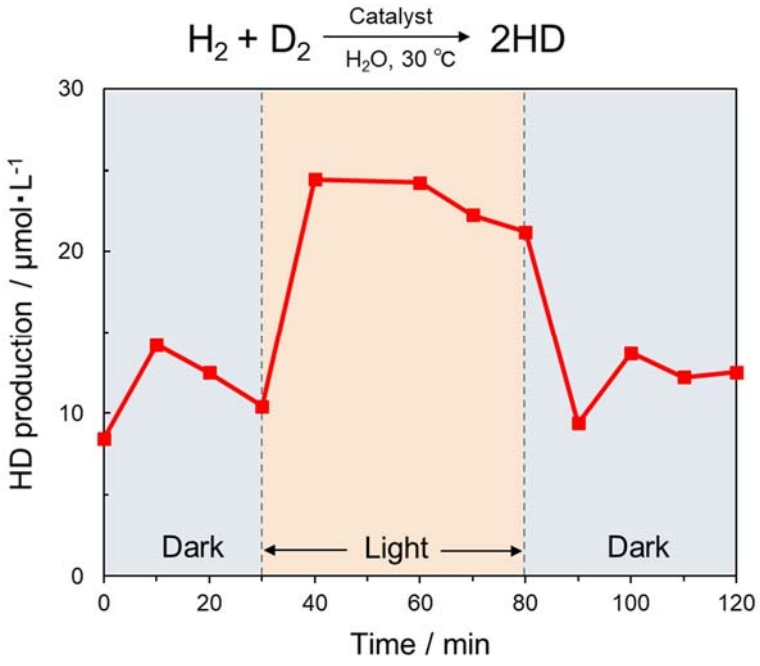

Figure 6 Time course in the HD formation from H_2 and D_2 over PdNPs/Au@rGO catalyst under visible light irradiation and in the dark.

4. Conclusion

In conclusion, a large SPR-mediated acceleration of H_2O_2 synthesis from H_2 and O_2 was obtained using the structure-controlled Pd-rGO-Au catalytic system. The synthesized nanocomposite catalyst was composed of the Au NR core and a rGO shell supporting the uniform Pd NPs with a mean diameter of 6.2 nm, which provided 3.5 times higher H_2O_2 production under visible light irradiation than in the dark after 30 min of reaction. The SPR of Au NRs drives the H_2 activation over the Pd NP surface, which leads to the promotion of H_2O_2 formation. This study is the first example of SPR-enhanced H_2O_2 production, and provides valuable insights into the design and application of plasmonic nanocomposite catalysts.

Acknowledgement

The present work was supported by Grants-in-Aid for Scientific Research (KAKENHI) (no. 19H00838) from the Japan Society for the Promotion of Science (JSPS). T.Y. thanks JSPS for a Research Fellowship for Young Scientists (no. 18J20246). This work was supported by Elements Strategy Initiative of MEXT (Grant no. JPMEXTP0112101003). A part of this work was supported in part by the Cooperative Research Program of "Network Joint Research Center for Materials and Devices" (no. 20191071). XAFS spectra were recorded at the BL01B1 station in SPring-8, JASRI, Harima, Japan (proposal nos. 2019B1091, 2019B1114). The authors appreciate Dr. Takashi Kamegawa at Osaka Prefecture University for his kind support in zeta potential measurement and Raman spectroscopy measurement.

References

[1] J.M. Campos-Martin, G. Blanco-Brieva, J.L.G. Fierro, Wasserstoffperoxid-Synthese: Perspektiven jenseits des Anthrachinon-Verfahrens, Angew. Chemie. 118 (2006) 7116–7139. https://doi.org/10.1002/ange.200503779.

[2] C. Samanta, Direct synthesis of hydrogen peroxide from hydrogen and oxygen: An overview of recent developments in the process, Appl. Catal. A Gen. 350 (2008) 133–149. https://doi.org/10.1016/j.apcata.2008.07.043.

[3] S. Melada, F. Pinna, G. Strukul, S. Perathoner, G. Centi, Direct synthesis of H2O2 on monometallic and bimetallic catalytic membranes using methanol as reaction medium, J. Catal. 237 (2006) 213–219. https://doi.org/10.1016/j.jcat.2005.11.008.

[4] I. Kumaniaev, J.S.M. Samec, Adsorption Isotherms of Lignin-Derived Compounds on a Palladium Catalyst, Ind. Eng. Chem. Res. 58 (2019) 6899–6906. https://doi.org/10.1021/acs.iecr.8b06159.

[5] F. Menegazzo, M. Signoretto, E. Ghedini, G. Strukul, Looking for the “Dream Catalyst” for Hydrogen Peroxide Production from Hydrogen and Oxygen, Catalysts. 9 (2019) 251. https://doi.org/10.3390/catal9030251.

[6] H. Xu, D. Cheng, Y. Gao, Design of High-Performance Pd-Based Alloy Nanocatalysts for Direct Synthesis of H2O2, ACS Catal. 7 (2017) 2164–2170. https://doi.org/10.1021/acscatal.6b02871.

[7] K. Nakatsuka, K. Mori, S. Okada, S. Ikurumi, T. Kamegawa, H. Yamashita, Hydrophobic modification of Pd/SiO2@single-site mesoporous silicas by triethoxyfluorosilane: Enhanced catalytic activity and selectivity for one-pot oxidation, Chem. - A Eur. J. 20 (2014) 8348–8354. https://doi.org/10.1002/chem.201402586.

[8] Y.F. Han, Z. Zhong, K. Ramesh, F. Chen, L. Chen, T. White, Q. Tay, S.N. Yaakub, Z. Wang, Au promotional effects on the synthesis of H2O2 directly from H2 and

O2 on supported Pd-Au alloy catalysts, J. Phys. Chem. C. 111 (2007) 8410–8413. https://doi.org/10.1021/jp072934g.

[9] A. Plauck, E.E. Stangland, J.A. Dumesic, M. Mavrikakis, Active sites and mechanisms for H 2 O 2 decomposition over Pd catalysts , Proc. Natl. Acad. Sci. 113 (2016) E1973–E1982. https://doi.org/10.1073/pnas.1602172113.

[10] J. Gu, S. Wang, Z. He, Y. Han, J. Zhang, Direct synthesis of hydrogen peroxide from hydrogen and oxygen over activated-carbon-supported Pd-Ag alloy catalysts, Catal. Sci. Technol. 6 (2016) 809–817. https://doi.org/10.1039/c5cy00813a.

[11] J. Zhang, B. Huang, Q. Shao, X. Huang, Highly Active, Selective, and Stable Direct H2O2 Generation by Monodispersive Pd-Ag Nanoalloy, ACS Appl. Mater. Interfaces. 10 (2018) 21291–21296. https://doi.org/10.1021/acsami.8b03756.

[12] I. Kim, M.G. Seo, C. Choi, J.S. Kim, E. Jung, G.H. Han, J.C. Lee, S.S. Han, J.P. Ahn, Y. Jung, K.Y. Lee, T. Yu, Studies on Catalytic Activity of Hydrogen Peroxide Generation according to Au Shell Thickness of Pd/Au Nanocubes, ACS Appl. Mater. Interfaces. 10 (2018) 38109–38116. https://doi.org/10.1021/acsami.8b14166.

[13] M. Manzoli, Boosting the Characterization of Heterogeneous Catalysts for H2O2 Direct Synthesis by Infrared Spectroscopy, Catalysts. 9 (2019) 30. https://doi.org/10.3390/catal9010030.

[14] U. Aslam, V.G. Rao, S. Chavez, S. Linic, Catalytic conversion of solar to chemical energy on plasmonic metal nanostructures, Nat. Catal. 1 (2018) 656–665. https://doi.org/10.1038/s41929-018-0138-x.

[15] W. Ye, R. Long, H. Huang, Y. Xiong, Plasmonic nanostructures in solar energy conversion, J. Mater. Chem. C. 5 (2017) 1008–1021. https://doi.org/10.1039/c6tc04847a.

[16] Y. Guo, J. Yu, C. Li, Z. Li, J. Pan, A. Liu, B. Man, T. Wu, X. Xiu, C. Zhang, SERS substrate based on the flexible hybrid of polydimethylsiloxane and silver colloid

decorated with silver nanoparticles, Opt. Express. 26 (2018) 21784-21796. https://doi.org/10.1364/OE.26.021784.

[17] J. Xu, C. Li, H. Si, X. Zhao, L. Wang, S. Jiang, D. Wei, J. Yu, X. Xiu, C. Zhang, 3D SERS substrate based on Au-Ag bi-metal nanoparticles/MoS 2 hybrid with pyramid structure, Opt. Express. 26 (2018) 21546-21557. https://doi.org/10.1364/OE.26.021546.

[18] J. Yu, Y. Guo, H. Wang, S. Su, C. Zhang, B. Man, F. Lei, Quasi Optical Cavity of Hierarchical ZnO Nanosheets@Ag Nanoravines with Synergy of Near- and Far-Field Effects for in Situ Raman Detection, J. Phys. Chem. Lett. 10 (2019) 3676–3680. https://doi.org/10.1021/acs.jpclett.9b01390.

[19] C. Zhang, C. Li, J. Yu, S. Jiang, S. Xu, C. Yang, Y.J. Liu, X. Gao, A. Liu, B. Man, SERS activated platform with three-dimensional hot spots and tunable nanometer gap, Sensors Actuators B Chem. 258 (2018) 163–171. https://doi.org/10.1016/j.snb.2017.11.080.

[20] C. Zhang, S.Z. Jiang, Y.Y. Huo, A.H. Liu, S.C. Xu, X.Y. Liu, Z.C. Sun, Y.Y. Xu, Z. Li, B.Y. Man, SERS detection of R6G based on a novel graphene oxide/silver nanoparticles/silicon pyramid arrays structure, Opt. Express. 23 (2015) 24811-24821. https://doi.org/10.1364/OE.23.024811.

[21] Y. Zhang, S. He, W. Guo, Y. Hu, J. Huang, J.R. Mulcahy, W.D. Wei, Surface-Plasmon-Driven Hot Electron Photochemistry, Chem. Rev. 118 (2018) 2927–2954. https://doi.org/10.1021/acs.chemrev.7b00430.

[22] J. Guo, Y. Zhang, L. Shi, Y. Zhu, M.F. Mideksa, K. Hou, W. Zhao, D. Wang, M. Zhao, X. Zhang, J. Lv, J. Zhang, X. Wang, Z. Tang, Boosting Hot Electrons in Hetero-superstructures for Plasmon-Enhanced Catalysis, J. Am. Chem. Soc. 139 (2017) 17964–17972. https://doi.org/10.1021/jacs.7b08903.

[23] A. Marimuthu, J. Zhang, S. Linic, Tuning Selectivity in Propylene Epoxidation

by Plasmon Mediated Photo-Switching of Cu Oxidation State, Science (80-.). 339 (2013) 1590–1593. https://doi.org/10.1126/science.1231631.

[24] X. Zhang, X. Li, D. Zhang, N.Q. Su, W. Yang, H.O. Everitt, J. Liu, Product selectivity in plasmonic photocatalysis for carbon dioxide hydrogenation, Nat. Commun. 8 (2017) 14542. https://doi.org/10.1038/ncomms14542.

[25] S. Mukherjee, L. Zhou, A.M. Goodman, N. Large, C. Ayala-Orozco, Y. Zhang, P. Nordlander, N.J. Halas, Hot-electron-induced dissociation of H2 on gold nanoparticles supported on SiO2, J. Am. Chem. Soc. 136 (2014) 64–67. https://doi.org/10.1021/ja411017b.

[26] S. Mukherjee, F. Libisch, N. Large, O. Neumann, L. V. Brown, J. Cheng, J.B. Lassiter, E.A. Carter, P. Nordlander, N.J. Halas, Hot Electrons Do the Impossible: Plasmon-Induced Dissociation of H 2 on Au, Nano Lett. 13 (2013) 240–247. https://doi.org/10.1021/nl303940z.

[27] T. Ming, L. Zhao, Z. Yang, H. Chen, L. Sun, J. Wang, C. Yan, Strong Polarization Dependence of Plasmon-Enhanced of plasmon-enhanced fluoresStrong polarization dependenccence on single gold nanorods. (SI), Nano Lett. 9 (2009) 3896–3903. https://doi.org/10.1021/nl902095q.

[28] T. Yoshii, Y. Kuwahara, K. Mori, H. Yamashita, Design of Pd–Graphene–Au Nanorod Nanocomposite Catalyst for Boosting Suzuki–Miyaura Coupling Reaction by Assistance of Surface Plasmon Resonance, J. Phys. Chem. C. 123 (2019) 24575–24583. https://doi.org/10.1021/acs.jpcc.9b06609.

[29] D.-K. Lim, A. Barhoumi, R.G. Wylie, G. Reznor, R.S. Langer, D.S. Kohane, Enhanced Photothermal Effect of Plasmonic Nanoparticles Coated with Reduced Graphene Oxide, Nano Lett. 13 (2013) 4075–4079. https://doi.org/10.1021/nl4014315.

[30] C. Matsubara, N. Kawamoto, K. Takamura, Oxo[5, 10, 15, 20-tetra(4-

pyridyl)porphyrinato]titanium(IV): An ultra-high sensitivity spectrophotometric reagent for hydrogen peroxide, Analyst. 117 (1992) 1781–1784. https://doi.org/10.1039/AN9921701781.

[31] Y. Isaka, Y. Kondo, Y. Kawase, Y. Kuwahara, K. Mori, H. Yamashita, Photocatalytic production of hydrogen peroxide through selective two-electron reduction of dioxygen utilizing amine-functionalized MIL-125 deposited with nickel oxide nanoparticles, Chem. Commun. 54 (2018) 9270–9273. https://doi.org/10.1039/C8CC02679C.

[32] L. Bai, X. Wang, Q. Chen, Y. Ye, H. Zheng, J. Guo, Y. Yin, C. Gao, Explaining the Size Dependence in Platinum-Nanoparticle-Catalyzed Hydrogenation Reactions, Angew. Chemie Int. Ed. 55 (2016) 15656–15661. https://doi.org/10.1002/anie.201609663.

[33] S. Ogo, K. Ichikawa, T. Kishima, T. Matsumoto, H. Nakai, K. Kusaka, T. Ohhara, A functional [NiFe]hydrogenase mimic that catalyzes electron and hydride transfer from H2, Science (80-.). 339 (2013) 682–684. https://doi.org/10.1126/science.1231345.

[34] K. Mori, Y. Futamura, S. Masuda, H. Kobayashi, H. Yamashita, Controlled release of hydrogen isotope compounds and tunneling effect in the heterogeneously-catalyzed formic acid dehydrogenation, Nat. Commun. 10 (2019) 4094. https://doi.org/10.1038/s41467-019-12018-7.

[35] Z. Zheng, T. Tachikawa, T. Majima, Plasmon-enhanced formic acid dehydrogenation using anisotropic Pd-Au nanorods studied at the single-particle level, J. Am. Chem. Soc. 137 (2015) 948–957. https://doi.org/10.1021/ja511719g.

[36] J. Guo, Y. Zhang, L. Shi, Y. Zhu, M.F. Mideksa, K. Hou, W. Zhao, D. Wang, M. Zhao, X. Zhang, J. Lv, J. Zhang, X. Wang, Z. Tang, Boosting Hot Electrons in Hetero-superstructures for Plasmon-Enhanced Catalysis, J. Am. Chem. Soc. 139 (2017) 17964–

17972. https://doi.org/10.1021/jacs.7b08903.

[37] W.S. Hummers, R.E. Offeman, Preparation of Graphitic Oxide, J. Am. Chem. Soc. 80 (1958) 1339. https://doi.org/10.1021/ja01539a017.

[38] S.Y. Liu, L. Huang, J.F. Li, C. Wang, Q. Li, H.X. Xu, H.L. Guo, Z.M. Meng, Z. Shi, Z.Y. Li, Simultaneous excitation and emission enhancement of fluorescence assisted by double plasmon modes of gold nanorods, J. Phys. Chem. C. 117 (2013) 10636–10642. https://doi.org/10.1021/jp4001626.

[39] Z. Çiplak, N. Yildiz, A. Çalimli, Investigation of Graphene/Ag Nanocomposites Synthesis Parameters for Two Different Synthesis Methods, Fullerenes, Nanotub. Carbon Nanostructures. 23 (2015) 361–370. https://doi.org/10.1080/1536383X.2014.894025.

[40] H.-J. Shin, K.K. Kim, A. Benayad, S.-M. Yoon, H.K. Park, I.-S. Jung, M.H. Jin, H.-K. Jeong, J.M. Kim, J.-Y. Choi, Y.H. Lee, Efficient Reduction of Graphite Oxide by Sodium Borohydride and Its Effect on Electrical Conductance, Adv. Funct. Mater. 19 (2009) 1987–1992. https://doi.org/10.1002/adfm.200900167.

[41] G.M. Lari, B. Puértolas, M. Shahrokhi, N. López, J. Pérez-Ramírez, Hybrid Palladium Nanoparticles for Direct Hydrogen Peroxide Synthesis: The Key Role of the Ligand, Angew. Chemie Int. Ed. 56 (2017) 1775–1779. https://doi.org/10.1002/anie.201610552.